Revista Brasileira de Geofísica
RBGf
Brazilian Journal of Geophysics

Revista Brasileira de Geofísica (2016) 34(4): 419-428

ISSN 0102-261X
www.scielo.br/rbg

ACOUSTIC TRAVELTIME TOMOGRAPHY FOR CO_2 INJECTION MONITORING IN RESERVOIRS

Luara Rodrigues Pereira[1] and Amin Bassrei[2]

ABSTRACT. When considering with greenhouse effect and global warming, carbon dioxide is the main agent. As the major contributors to the increase in global temperature, large companies and corporations have been encouraged to look for ways to reduce the emission of CO_2 into the atmosphere. In the geological aspect, two techniques have been applied in the use of CO_2. The first is the carbon capture and storage, CCS, which refers to carbon dioxide injection into saline aquifers, reservoirs and coal deposits, helping to limit CO_2 emissions. The second is the enhanced oil recovery, or EOR, which refers to the injection of CO_2 in heavy oil reservoirs to decrease the viscosity and increase the recovery factor. Because CO_2 can interact with rock, changing its porosity or changing the direction of flow due to lower permeability zones, periodic monitoring of CO_2 must be performed. In this work, methods of dealing with the poor conditioning of the inverse problem were discussed, applying the methods of singular value decomposition and ray tracing. The Gassmann equation was used to simulate the velocity change within the reservoir due to fluid substitution. The above methods were incorporated into traveltime seismic tomography, which was applied to monitor the carbon dioxide injection in reservoirs. Several simulations in a synthetic model validated the proposed methodology.

Keywords: traveltime tomography, reservoir monitoring, geological storage, CO_2 injection.

RESUMO. Quando tratamos do efeito estufa e aquecimento global temos como seu principal agente o dióxido de carbono. Por serem grandes contribuintes do aumento da temperatura do planeta, grandes empresas e corporações têm sido incentivadas a buscar formas de reduzir a emissão de CO_2 na atmosfera. No aspecto geológico, duas técnicas têm sido aplicadas no aproveitamento do CO_2. A primeira é o armazenamento geológico de CO_2 ou CCS, do inglês *carbon capture and storage*, que trata da injeção de dióxido de carbono em aquíferos salinos, reservatórios e camadas de carvão, ajudando a limitar a emissão de CO_2. A segunda é a recuperação avançada de petróleo ou EOR (do inglês *enhanced oil recovery*), que se refere à injeção de CO_2 em reservatório de óleo pesado com o intuito de diminuir a viscosidade e aumentar seu fator de recuperação. Devido ao fato do CO_2 poder interagir com a rocha, alterando sua porosidade ou mudando a direção do fluxo devido a regiões de menor permeabilidade, é necessário realizar um monitoramento periódico do CO_2. Neste trabalho foram abordadas formas de lidar com o mau condicionamento do problema inverso, onde aplicamos o método de decomposição em valores singulares juntamente com o traçado de raios. Utilizou-se a equação de Gassmann para simular a variação da velocidade dentro do reservatório devido a uma substituição de fluidos. As técnicas acima foram incorporadas à tomografia sísmica de tempos de trânsito para o monitoramento da injeção do dióxido de carbono nos reservatórios. As diversas simulações num modelo sintético validaram a metodologia proposta.

Palavras-chave: tomografia de tempos de trânsito, monitoramento de reservatórios, armazenamento geológico, injeção de CO_2.

[1]Universidade Federal da Bahia, Institute of Geosciences – E-mail: luara.r.pereira@gmail.com

[2]Universidade Federal da Bahia, Research Center in Geophysics and Geology, Institute of Geosciences and National Institute of Science and Technology in Petroleum Geophysics, Rua Barão de Jeremoabo, s/n, Ondina, 40170-115, Salvador, BA, Brazil. Phone: +55(71) 3283-8508 – E-mail: bassrei@ufba.br

INTRODUCTION

Recently, one of the industries that has most mobilized in an attempt to encourage research to develop more appropriate management of greenhouse gas emissions (including CO_2) is the oil industry. One of the alternatives studied and applied is carbon capture and storage (CCS), which occurs preferentially in natural reservoirs, where there is almost no risk of impact on human consumption. CO_2 sequestration involves carbon dioxide injection into saline aquifers, reservoirs and coal deposits, helping to limit CO_2 emissions and enabling the continued use of fossil energy sources to provide more time for the transition to sustainable energy systems.

A common practice in the oil industry is fluid injection technique enhanced oil recovery (EOR). This practice has been used in carbon sequestration. Some depleted reservoirs also contain large quantities of oil, which can be produced by the injection of CO_2, a fluid capable of reactivating the production, with the benefits of reducing the cost of injection while at the same time mitigating the impact of CO_2 emission to the atmosphere (Ravagnani & Suslick, 2008). In addition, preference is given to oil and gas reservoirs for CO_2 sequestration because they are long-term proven traps for fluids and gases with known geological parameters with immediate availability and considerable potential. When injected into a reservoir, the carbon dioxide may behave in different ways. It can interact with the reservoir rocks (when we are dealing with carbonate rocks) increasing or decreasing their porosity, and can change the direction of flow due to lower permeability regions. Thus, it is necessary to conduct periodic monitoring of CO_2.

Geophysical analysis is an essential tool both in geological sequestration of CO_2 and for an enhanced oil recovery, starting with the choice of target reservoirs for permanent storage of carbon dioxide (in the case of sequestration) and extending to the monitoring of its integrity. Of the existing geophysical methods, seismic analysis is the most used for the selection of targets and monitoring. However, other methods can be employed during monitoring, preferably in an integrated manner, such as electromagnetic, gravimetric and electrical methods. For this work, we propose the use of traveltime seismic tomography to map the velocity changes resulting from the injection of carbon dioxide in a reservoir.

Tomography is classified as traveltime tomography, which has a cinematic approach because it considers the travel time between sources and receivers of the transmitted or reflected wave, and waveform tomography, which considers the waveform of the signal that gets to the receiver. The tomographic inversion is an ill-posed problem because the conditions of existence, unity and stability are not completely satisfied. To numerically solve such problems, mathematical techniques are applied to obtain a better conditioning.

In this work we discuss options of dealing with the ill-conditioning of the inverse problem. The method of singular value decomposition with regularization is applied to achieve better results to study the viability of traveltime seismic tomography in the monitoring of CO_2 in saline reservoirs based on synthetic models.

This article is divided as follows: first, an overview of inversion theory, the selection of single values and the regularization by derivative matrices is presented. Second, the Gassmann equation showing the effects of a substitution fluid in a reservoir is introduced. Third, a brief introduction to the theory of seismic traveltime tomography is presented. Finally, the results of numerical simulations for different stages of CO_2 saturations in the studied reservoir are presented and discussed.

INVERSE PROBLEMS AND LINEARIZED INVERSION

Geophysics studies the physical characterization of subsurface areas based on data recorded in the subsurface of the earth. The inversion technique is used for such situations to estimate the parameters of a particular model from the input data. Conversely, the direct modeling technique results in a synthetic model for obtaining these data.

The description of the geophysical data is the initial step in the analysis, where the most practical means of representing these values is through vectors. Thus,

$$\mathbf{d} = [d_1, d_2, d_3, d_4, \ldots, d_M]^T$$

is the data observed and

$$\mathbf{m} = [m_1, m_2, m_3, m_4, \ldots, m_N]^T$$

is the model. The equation $\mathbf{d} = \mathbf{Gm}$ is the physical/mathematical solution of the problem called direct modeling, which means that for a given model, $\mathbf{m}$, we can calculate $\mathbf{d}$ when it consists of a linear combination of independent functions.

The method of ordinary least squares consists of a solution where the sum of squared errors is minimal. If we consider modeling a process where $\mathbf{m}$ is a vector of model parameters, the output is given by $\mathbf{Gm} = \mathbf{d}$. The vector $\mathbf{d}$ describes the real observed behavior. The difficulty is to select the parameters $\mathbf{m}$ to minimize the difference between $\mathbf{Gm}$ and $\mathbf{d}$, i.e., the error $\mathbf{e} = \mathbf{d} - \mathbf{Gm}$, whose measure is given by $\|\blacksquare\|$. As a linear system, $\mathbf{d} = \mathbf{Gm}$, the sum of squared errors is given by the objective function or cost function:

$$S(\mathbf{m}) = \|\mathbf{e}\|^2 = \mathbf{d}^T\mathbf{d} - 2\mathbf{m}^T\mathbf{G}^T\mathbf{d} + \mathbf{m}^T\mathbf{G}^T\mathbf{Gm}. \quad (1)$$

Equation (1) corresponds to the equation of a paraboloid with no negative values having a single minimum point. This minimum point, $\mathbf{m}^*$ is associated with the parameters that cancel the derivative:

$$\frac{\partial S(\mathbf{m})}{\partial \mathbf{m}^T}|_{\mathbf{m}=\mathbf{m}^*} = \mathbf{0}. \quad (2)$$

Solving the system of equations obtained for m we have the ordinary least squares solution:

$$\mathbf{m} = (\mathbf{G}^T\mathbf{G})^{-1}\mathbf{G}^T\mathbf{d}. \quad (3)$$

The matrix $(\mathbf{G}^T\mathbf{G})^{-1}\mathbf{G}^T$ in equation (3) can be calculated using the generalized inverse technique. The determination of $\mathbf{m}$, the model that best describes the observed data, is called the inverse problem.

The parameters of the Earth model usually relate non-linearly with the geophysical observed data. The equivalent representation of $\mathbf{d} = \mathbf{G}\mathbf{m}$ for the non-linear case is given by $\mathbf{d} = g(\mathbf{m})$.

In the linearized inversion method we start from an initial model, $\mathbf{m}_o$, which is reformulated successively. This is also known as the Gauss-Newton method, which linearizes the non-linear problem $g(\mathbf{m}) = \mathbf{d}$ around an approximate solution. The estimation of the model is obtained iteratively by solving a system of equations for each step of the iterative process. The method converges to the model associated with the minimum of the cost function closest to $S(\mathbf{m}_o)$, so the obtainment of the global minimum, $S(\mathbf{m}^{est})$, strongly depends on the initial model.

Deviations used in the generation of the cost function are given by,

$$\Delta d_i = d_i^{obs} - g(\mathbf{m}, d_i), \qquad i = 1, \ldots, M. \quad (4)$$

where $\Delta\mathbf{d}^k = \mathbf{d}^k - \mathbf{G}^k\Delta\mathbf{m}^k$ is the vector notation of equation (4), and $\mathbf{m}^k = (m_1^k, \ldots, m_N^k)^T$ is the current model. We can obtain an expression to update the current model:

$$(\mathbf{G}^T\mathbf{G})^k\Delta\mathbf{m}^k = \mathbf{G}^{k,T}\Delta\mathbf{d}^k, \quad (5)$$

$$\mathbf{m}^{k+1} = \mathbf{m}^k + (\mathbf{G}^T\mathbf{G})^{k,+}G^{k,T}\Delta\mathbf{d}^k, \quad (6)$$

where $\Delta\mathbf{m}^k$ is the estimated update of the model parameters, $(\mathbf{G}^T\mathbf{G})^{k,+}$ is the pseudo-inverse matrix of $(\mathbf{G}^T\mathbf{G})^k$, $\mathbf{m}^k$ are the current parameters of the model in k-th iteration, $\Delta\mathbf{d}^k$ is the difference between the data of iteration $k+1$ and the data of the k-th iteration, and $\mathbf{m}^{k+1}$ are the estimated parameters for the iteration $k+1$. The above algorithm is known as the Gauss-Newton method.

SINGULAR VALUES AND REGULARIZATION

Geophysical problems are usually represented by rectangular matrices, so an inverse matrix does not exist. Therefore, one can determine the pseudo-inverse of a matrix $\mathbf{G}$ using singular value decomposition or SVD. This consists of determining two orthogonal matrices and the singular eigenvalue matrix from the matrix $\mathbf{G}$, satisfying the following condition:

$$\mathbf{G} = \mathbf{U}\mathbf{\Sigma}\mathbf{V}^T, \quad (7)$$

where $\mathbf{U}$ and $\mathbf{V}$ are orthonormal matrices and $\mathbf{\Sigma}$ is a diagonal matrix having singular values of $\mathbf{G}$. Given a $\mathbf{\Sigma}_{M\times N}$, matrix, there are orthogonal matrices $\mathbf{U}_{M\times M}$ and $\mathbf{V}_{N\times N}$, that combine with $\mathbf{\Sigma}_{M\times N}$ matrix to produce the result mentioned above.

Then, based on equation (7) and the orthonormality property, one can determine the generalized inverse or pseudo-inverse $\mathbf{G}^+$ of $\mathbf{G}$ using singular value decomposition:

$$\mathbf{G}^+ = \mathbf{V}\mathbf{\Sigma}^+\mathbf{U}^T. \quad (8)$$

One way to make the solution of the problem more stable is minimally limiting the variation of the model parameters. The difference between the parameters of the model can be used as an approximation of the first derivative. The sum of these values can be defined as the flatness $\mathbf{l}_1$ (Menke, 1989) of the vector solution $\mathbf{m}$,

$$\mathbf{l}_1 = \begin{bmatrix} -1 & 1 & 0 & \ldots & 0 & 0 & 0 \\ 0 & -1 & 1 & 0 & \ldots & 0 & 0 \\ \vdots & \vdots & \vdots & \ddots & \vdots & \vdots & \vdots \\ 0 & 0 & 0 & \ldots & 0 & -1 & 1 \end{bmatrix} \begin{bmatrix} m_1 \\ m_2 \\ \ldots \\ m_N \end{bmatrix} = \mathbf{D}_1\mathbf{m}. \quad (9)$$

The roughness $\mathbf{l}_2$ of the model parameters can be determined using an approximation of the matrix of the second derivative $\mathbf{D}_2$:

$$\mathbf{l}_2 = \begin{bmatrix} 1 & -2 & 1 & 0 & \ldots & 0 & 0 & 0 & 0 \\ 0 & 1 & -2 & 1 & \ldots & 0 & 0 & 0 & 0 \\ \vdots & \vdots & \vdots & \vdots & \ddots & \vdots & \vdots & \vdots & \vdots \\ 0 & 0 & 0 & 0 & \ldots & 0 & 1 & -2 & 1 \end{bmatrix} \begin{bmatrix} m_1 \\ m_2 \\ \ldots \\ m_N \end{bmatrix} = \mathbf{D}_2\mathbf{m}. \quad (10)$$

The L_n value of flatness $(n = 1)$ or roughness $(n = 2)$ of the vector $\mathbf{m}$ is calculated by:

$$L_n = \|\mathbf{l}_n\|_2^2 = (\mathbf{D}_n\mathbf{m})^T(\mathbf{D}_n\mathbf{m}), \tag{11}$$

where n is the order of the derivative of the matrix. An objective function $\Phi(\mathbf{m})$ can be defined:

$$\Phi(\mathbf{m}) = \mathbf{e}^T\mathbf{e} + \lambda L_n. \tag{12}$$

By replacing $\mathbf{e} = \mathbf{d} - \mathbf{G}\mathbf{m}$ and $\mathbf{L}_n$ in equation (12), we obtain:

$$\Phi(\mathbf{m}) = (\mathbf{d} - \mathbf{G}\mathbf{m})^T(\mathbf{d} - \mathbf{G}\mathbf{m}) + \lambda(\mathbf{D}_n\mathbf{m})^T(\mathbf{D}_n\mathbf{m}), \tag{13}$$

where λ is a positive constant called the regularization parameter, which is the intensity of the regularization value to be applied to obtain a satisfactory solution. When $\lambda = 0$, the equation lies in the method of ordinary least squares, and when it has a value of $\lambda \neq 0$ and the order of the derivative is zero, we have an identity matrix. Therefore, the solution lies in the damped least squares method.

Minimizing the objective function presented in equation (13) and equating its result to zero, we find the solution $(\mathbf{m}^{est})$ that produces the smallest error:

$$\mathbf{m}^{est} = (\mathbf{G}^T\mathbf{G} + \lambda\mathbf{D}_n{}^T\mathbf{D}_n)^{-1}\mathbf{G}^T\mathbf{d}. \tag{14}$$

GASSMANN'S EQUATION

The Gassmann equation can model various scenarios with different fluid types and fluid saturations. The equation relates the bulk modulus (K) of the rock through the pore, frame and fluid properties:

$$K_{sat} = K_{dry} + \frac{\left(1 - \frac{K_{dry}}{K_{\min}}\right)^2}{\frac{\phi}{K_{fluid}} + \frac{(1-\phi)}{K_{\min}} - \frac{K_{dry}}{K_{\min}^2}}, \tag{15}$$

where K_{sat} is the bulk modulus of a saturated rock with a fluid of bulk modulus K_{fluid}, K_{dry} is the bulk modulus of dry rock, $K_{\min}$ is the bulk modulus of the mineral and ϕ is the rock porosity.

The shear modulus is not affected by the presence of fluid, so:

$$\mu_{sat} = \mu_{dry}, \tag{16}$$

where μ_{sat} is the shear modulus of the saturated rock and μ_{dry} is the shear modulus of dry rock. The density of the saturated rock and the density of the dry rock are given, respectively, by:

$$\rho = (1 - \phi)\rho_{\min} + \phi\rho_{fluid} \tag{17}$$

and

$$\rho_{dry} = (1 - \phi)\rho_g. \tag{18}$$

The fluid density is calculated by the following equation:

$$\rho_{fl} = S_a\rho_a + S_o\rho_o + S_g\rho_g, \tag{19}$$

where S_a, S_o and S_g are the water, oil and gas saturation, and ρ_a, ρ_o and ρ_g are the water, oil and gas densities, respectively.

Gassmann's equation is based on various assumptions (Wang, 2001): (i) the rock is uniform and isotropic, and the pore space is completely connected; (ii) the rock is composed of a single type of mineral; (iii) the equation is valid for low frequencies; and (iv) the fluid does not interact with the rock. Smith et al. (2003) showed that the bulk modulus of a rock composed of a single type of mineral can be calculated from the Hill's average.

From the saturated rock bulk modulus modeled with the Gassmann equation we can estimate the velocity of the saturated reservoir for any type of fluid:

$$v_p = \sqrt{\frac{K_{sat} + \frac{3}{4}\mu}{\rho}}. \tag{20}$$

We know that the Gassmann equation can model the velocity expected for a reservoir that suffers a certain change in fluid saturation. However, it is important to know which factors influence in the seismic velocity inside the reservoir, enabling the understanding of the modeling.

Some of the main factors affecting the value of the seismic velocity in the reservoir are: the type of fluid, fluid saturation, rock type, porosity, the pressure to which the reservoir is subjected, the pore pressure, the ratio of sandstone and clay, and the relationship between age and depth. Some factors are static, such as rock type and the volume of clay, whereas others vary depending on the exploitation of the reservoir and the type of fluid being injected, in addition to the pressure with which the fluid is being injected and/or exploited. Thus, there may be variation in the porosity of a reservoir. The injection of CO_2 into carbonate reservoirs is one example. When CO_2 is injected into a reservoir, it will react with water, causing mineral precipitation in some regions and mineral deposition in others, modifying the porosity of the formation.

SEISMIC TRAVELTIME TOMOGRAPHY

Tomography is based on the idea that a set of observed data consists of integrals along lines of some physical quantity. Thus, the traveltime of the energy that propagates through the Earth's interior section, considering that it was discretized on N rectangular

cells and M pairs of source-receptor distribution, is:

$$t_i = \sum_{j=1}^{N} g_{ij} s_j, \qquad i = 1, \ldots, M. \tag{21}$$

The tomographic reconstruction in terms of line integral is given by:

$$t_i = \int_{R_i} s(x,z) dl = g_i[s(x,z)], \tag{22}$$

where t_i is the traveltime for the i-th radius, R_i is the radius along which the integration is performed, dl is the distance element $s(x,z)$ is the slowness in the middle of the point (x,z), where x is the horizontal coordinate and z is the vertical coordinate and $g[s(x,z)]$ is the variable g as a function of slowness. Equation (22) has nonlinear behavior because it describes the ray path in an inhomogeneous and anisotropic environment, providing complex ray geometry. Therefore, it is necessary to use the linearization method described previously.

Starting from an initial model, we can calculate the value for new slowness by an iterative process.

$$\Delta \mathbf{s}^k = (\mathbf{G}^T \mathbf{G})^{k,+} \mathbf{G}^{k,T} \Delta \mathbf{t}^k, \tag{23}$$

to update the slowness:

$$\mathbf{s}^{k+1} = \mathbf{s}^k + \Delta \mathbf{s}^k. \tag{24}$$

where $\Delta \mathbf{t}$ corresponds to the vector difference between the calculated and observed traveltimes for the model, $\Delta \mathbf{s}$ is the vector corresponds to the difference between true and estimated slowness model, and $\mathbf{G}$ is the matrix that contains the elements g_{ij} corresponding to the distances that the i-th ray travels in the j-th block.

FORWARD MODELING BY RAY TRACING

The seismic signals propagating in a medium can be represented in various ways: analytical models, finite difference, and ray tracing. Modeling using ray tracing gives us accuracy, along with computational efficiency when modeling geological media.

In the geometric acoustic approach, energy can be regarded as being transported along curved trajectories that are orthogonal to the movement of the wavefront. A more logical way of analyzing ray tracing without the concept of the wavefront is the principle of Fermat. The principle states that energy propagates along paths that minimize the traveltime. This path is called ray (Andersen & Kak, 1982) and it is used to calculate the integral:

$$I = \int_{p1}^{p2} n(x,z) ds. \tag{25}$$

Equation (25) defines the acoustic length between the points p_1 and p_2 along the ray, $n(x,z) = c/v(x,z)$ is the two-dimensional refractive index corresponding to the position (x,z) in a heterogeneous isotropic medium, and ds is the arc length along the ray.

Several methods are described in the literature to determine the path described by the distance between two points. The following is the numerical algorithm described by Schots (1990). Applying the principle of Fermat in equation (22) and knowing that the Euler equation is a necessary condition for the existence of an extreme value of the integral $\int_{p1}^{p2} n ds$, we obtain the following differential equation for a heterogeneous environment:

$$\frac{d}{ds}\left(n \frac{d\mathbf{r}}{ds}\right) = \nabla n, \tag{26}$$

where $n(x,z)$ is the refractive index at position (x,z), $\mathbf{r}$ is the ray position vector, $d\mathbf{r}$ is the vector tangential to the ray in (x,z), ds is the ray path length element, and $\nabla n \equiv dn/d\mathbf{r}$ is the gradient of the refractive index $n(x,z)$. This differential equation is called the ray equation, and for a certain neighborhood (in which the refractive index varies smoothly), its solution represents a family of smaller acoustic ray lengths (Andersen & Kak, 1982).

Developing the ray equation, we obtain:

$$\frac{dn}{ds}\frac{d\mathbf{r}}{ds} + n\frac{d^2\mathbf{r}}{ds^2} = \nabla n. \tag{27}$$

But,

$$\frac{dn}{ds} = \frac{dn}{d\mathbf{r}} \cdot \frac{d\mathbf{r}}{ds} = \nabla n \cdot \frac{d\mathbf{r}}{ds}\,, \tag{28}$$

then,

$$\left(\nabla n \cdot \frac{d\mathbf{r}}{ds}\right)\frac{d\mathbf{r}}{ds} + n\frac{d^2\mathbf{r}}{ds^2} = \nabla n\,. \tag{29}$$

Taking into account two distinct points of the ray, $P_1(x_k, z_k)$ and $P_2(x_{k+1}, z_{k+1})$ separated by a distance Δs, the unit vector in the propagation direction can be written as:

$$\frac{d\mathbf{r}}{ds} = (\cos\alpha_k)\hat{\imath} + (\sin\alpha_k)\hat{k}\,, \tag{30}$$

where $\hat{\imath}$ and $\hat{k}$ are the unit vectors in the x and z directions, respectively, and the angle between the tangent and the horizontal directions in iteration k is α_k. The values of the sine and cosine can be obtained by:

$$\sin\alpha_k = \frac{z_{k-1} - z_k}{\Delta s}\,, \tag{31}$$

$$\cos\alpha_k = \frac{x_{k-1} - x_k}{\Delta s}\,. \tag{32}$$

Through finite difference, we can approach the directional derivatives from the discretized media by:

$$n_x(i,j) = \frac{n(i+1,j) - n(i-1,j)}{2\Delta x}, \tag{33}$$

$$n_z(i,j) = \frac{n(i,j+1) - n(i,j-1)}{2\Delta z}. \tag{34}$$

The next point in the ray is estimated by the equation:

$$x_{k+1} = x_k + \cos\alpha_k \Delta s + \frac{1}{2n_k}(n_{k,x} - d_k \cos\alpha_k)\Delta s^2, \tag{35}$$

and

$$z_{k+1} = z_k + \sin\alpha_k \Delta s + \frac{1}{2n_k}(n_{k,z} - d_k \sin\alpha_k)\Delta s^2, \tag{36}$$

where n_k, $n_{k,x}$ and $n_{k,z}$ are, respectively, the refractive index and the directional derivative in the x and z directions. For equations (35) and (36), the substitution $n_k = c/v_k = cs_k$ was made, where s_k is the slowness and v_k is the velocity. Finally, the equations (35) and (36) can be written as:

$$x_{k+1} = x_k + \cos\alpha_k \Delta s + \frac{1}{2s_k}(s_{k,x} - d_k \cos\alpha_k)\Delta s^2, \tag{37}$$

and

$$z_{k+1} = z_k + \sin\alpha_k \Delta s + \frac{1}{2s_k}(s_{k,z} - d_k \sin\alpha_k)\Delta s^2, \tag{38}$$

and d_k is defined as:

$$d_k = s_{k,x}\cos\alpha_k + s_{k,z}\sin\alpha_k. \tag{39}$$

Beginning from a given starting point (x_0, z_0), corresponding to the source position, successive points in the ray can be obtained because the values of $\sin\alpha_k$ and $\cos\alpha_k$ are calculated by equations (31) and (32). According to Andersen & Kak (1982), this method has some limitations due to the fact the errors from discretization and sudden velocity transitions, may become accumulative. To minimize this problem, a grid with sufficient resolution is adopted so that the medium is sampled appropriately, resulting in smoother velocity transitions.

NUMERICAL SIMULATIONS

The geological model of the study is inspired by the Miranga Field in the Reconcavo Basin. Four phases of monitoring were simulated. The first is at a stage where the injection of CO_2 has not occurred and the subsequent phases have the presence of carbon dioxide injected into the reservoir gradually. The model on which the simulations are conducted was parameterized in a 30×30 grid totaling 900 blocks with dimensions of 20 m. The acquisition geometry used is well-to-well, where 30 sources were arranged in the left-side borehole and 30 receivers were located in the right-side borehole. Different stages of CO_2 saturation are applied to the reservoir initially saturated with water. In Table 1, we observe the main properties that affect the seismic velocity in the reservoir.

Table 1 – Reservoir properties during injection, where S_{H2O} is the water saturation, S_{CO2} is the CO_2 saturation, K_{CO2} is the bulk modulus of CO_2, K_{sat} is the bulk modulus of the saturated rock, ρ_{sat} is the density of the saturated rock and V_p is the P wave velocity. The water density is 1.0 g/cm^3, and the bulk modulus of water is 2.25 GPa.

Reservoir properties during injection						
S_{H2O}	S_{CO2}	K_{CO2}	K_{sat}	ρ_{CO2}	ρ_{sat}	V_p
100%	0%	0.25	12.8	0.71	2.14	2930
70%	30%	0.25	8.85	0.71	2.1	2610
40%	60%	0.25	8.81	0.71	2.09	2560

Two methods were used to compensate the ill-posed condition of the inverse problem used. The first consisted of a variable selection of singular values associated to different condition numbers, to have greater control of the outcome of the experiment. The second method used is the regularization by derivative matrices of zero, first order and second orders. The data parameters (traveltimes) were corrupted by Gaussian noise, and three noise levels were used in the simulations, given by the noise factor a: 0.005, 0.01 and 0.05.

In the first stage (see Fig. 1), carbon dioxide injection into the reservoir has not yet occurred, and the reservoir is saturated with water. This stage is used to understand the geological context of the area, to compare the results, and to analyze the behavior CO_2 within the reservoir. For the injection of fluid, the upper reservoir was used. This layer is considered to be composed of quartz, feldspar and clay in proportions of 65%, 20% and 15%, respectively.

The use of traveltime tomography resulted in the following results for the first stage: 658 singular values were used for the solution of the linear inverse problem. By using a large amount of numbers, it was possible to obtain the model framework, except when there is relatively high noise (see Fig. 2). In the regularization process by derivative matrices, the estimated tomogram

quality decreases as the noise level increases. This influence is strongest in the regularization of zero order (see Fig. 3), where the retrieved image does not provide information about the true model for the highest noise. The regularization of the first and second orders (see Fig. 4) provided the best results by performing a mitigation without significantly increasing the error in the model estimation.

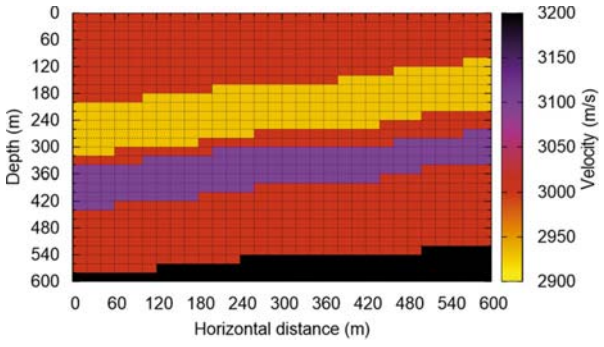

Figure 1 – True model, first stage with 100% saturation of water in the reservoir of interest with $V_p = 2930$ m/s.

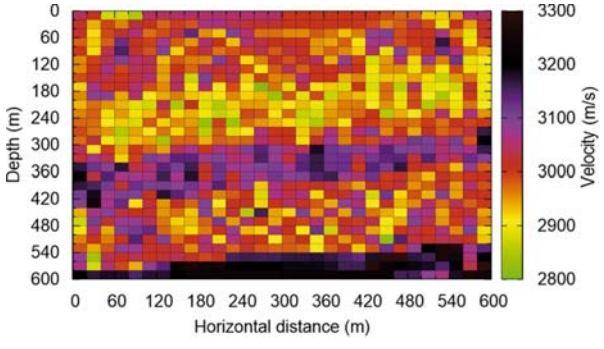

Figure 2 – Estimated model, linear case, first stage with 658 singular values and noise factor $\alpha = 0.005$.

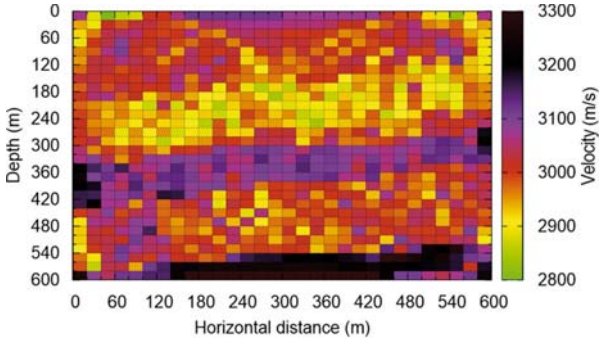

Figure 3 – Estimated model, linear case, first stage with zero order regularization and noise factor $\alpha = 0.005$.

For the linearized inversions 500 singular values were used, adding different levels of noise to the observed data. As expected, the model error is reduced in each iteration, even with the increase of the noise factor, converging, approximately, at the fourth interaction (see Fig. 5). For regularization, even when the estimated model image is diffuse, the image suggests velocities approaching of the real image model (see Fig. 6).

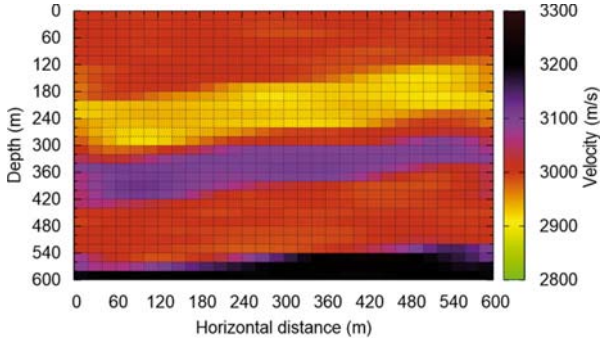

Figure 4 – Estimated model, linear case, first stage with first order regularization and noise factor $\alpha = 0.005$.

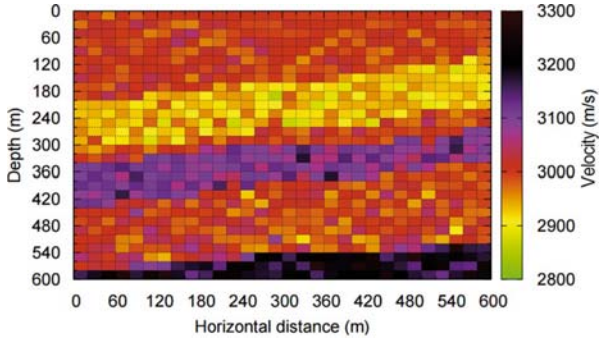

Figure 5 – Estimated model, linearized case, fourth interaction of the first stage with 500 singular values and noise factor $\alpha = 0.005$.

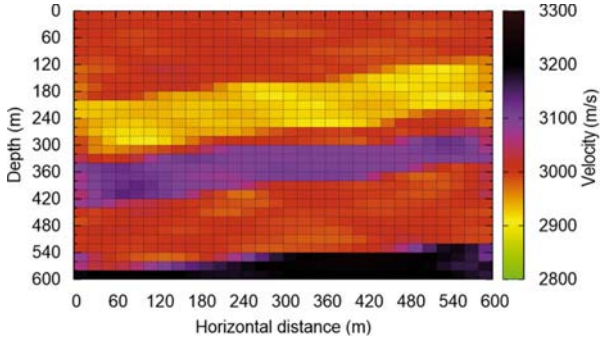

Figure 6 – Estimated model, linearized case, fourth interaction of the first stage with first order regularization and noise factor $\alpha = 0.005$.

The second stage (see Fig. 7) begins the injection of carbon dioxide at the left side of the model. After the start of injection, part of the reservoir is saturated with 30% CO_2 and the rest remains saturated with 100% water. A visual analysis of the estimated model, obtained from the selection of singular values for the linear case, shows that the saturated region with 30% CO_2 can

be easily viewed. By applying regularization, the estimated tomograms quality decreases as they the noise level increases. This influence is most effectively recorded in the regularization of zero order. However, adjustments to orders one and two (see Fig. 8) provided to be the best results.

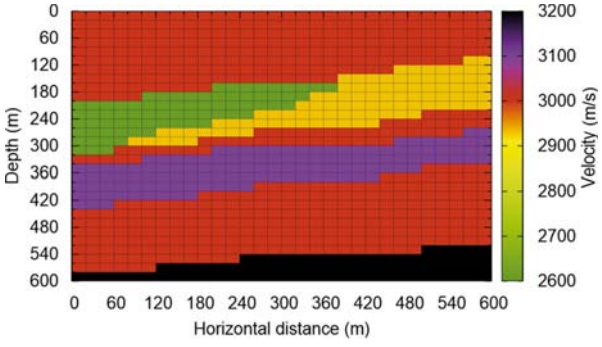

Figure 7 – True model, second stage, with saturation of 30% CO_2 in the green region of the reservoir of interest.

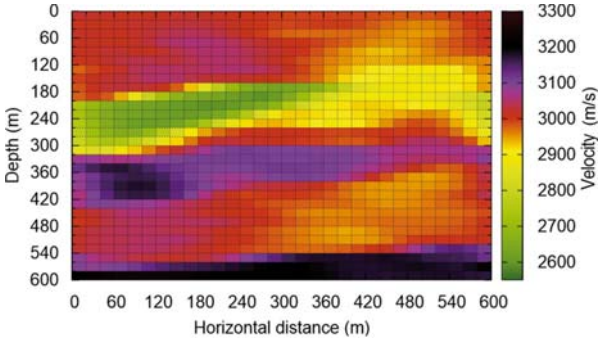

Figure 8 – Estimated model, linear case, second stage with first order regularization and noise factor $\alpha = 0.010$.

In the linearized case, the estimated model converges on the fourth interaction for the selection of singular values, as well as the regularization. In both cases, the position of layers and the velocities suggest that the image approximates the true model, showing a good delimitation, especially in the fourth interaction, for the region in which the fluid is located (see Fig. 9).

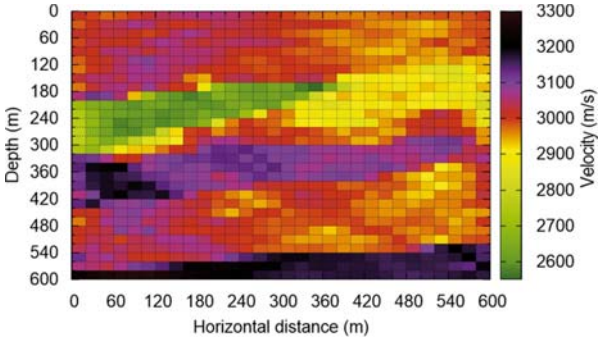

Figure 9 – Estimated model, linearized case, second stage with first order regularization and noise factor $\alpha = 0.010$.

The third stage shows the condition of the reservoir after another carbon dioxide injection period. CO_2 has mobility such that it is assumed that in this stage, it is divided into three regions of different saturations and seismic velocities (see Fig. 10). The region that was previously saturated with 30% CO_2 and 70% water has its CO_2 saturation increased to 60%. The middle of the reservoir has a region with 30% CO_2 saturation followed by a region of 100% water.

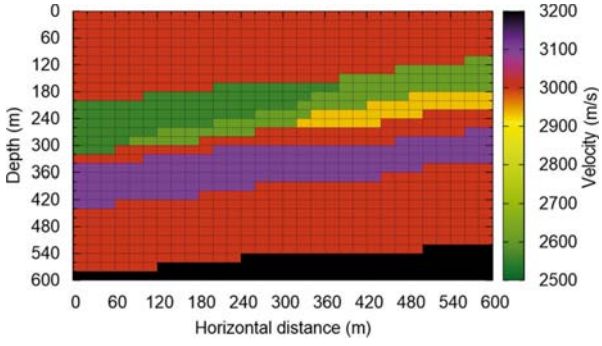

Figure 10 – True model, third stage with different levels of CO_2 and water saturation in the reservoir of interest.

Figure 11 shows the model estimated for the selection of singular values in the linear case, which allows us to visualize saturated regions with 30% and 60% CO_2. However, because the two regions are represented by different shades of green, the distinction between them is unclear. The regularization provides satisfactory results because they delimit the region where the CO_2 is located, but the distinction of regions of different saturation only occurs in the regularization of the zero order and is subtly noted in the first order (see Fig. 12).

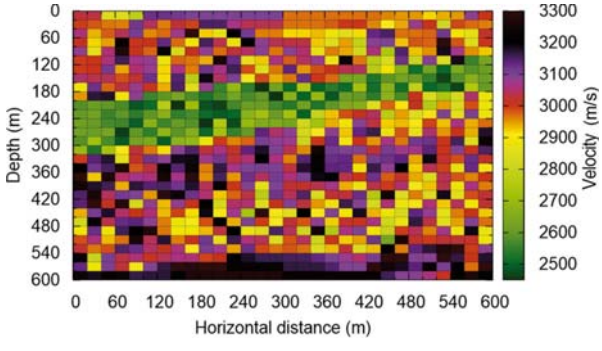

Figure 11 – Estimated model, linear case, third stage with 300 singular values and noise factor $\alpha = 0.010$.

In linearized inversion, it is possible to effectively define the saturated region with CO_2, in both forms of conditioning of the inverse problem. For all regularization orders, even when the image of the estimated model is not as clear because of the dispersion of energy, it was possible to view, especially in the fourth interaction, the region where the CO_2 is located (see Fig. 13).

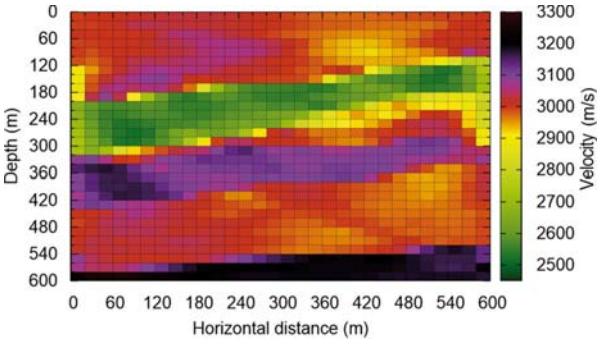

Figure 12 – Estimated model, linear case, third stage with first order regularization and noise factor $\alpha = 0.010$.

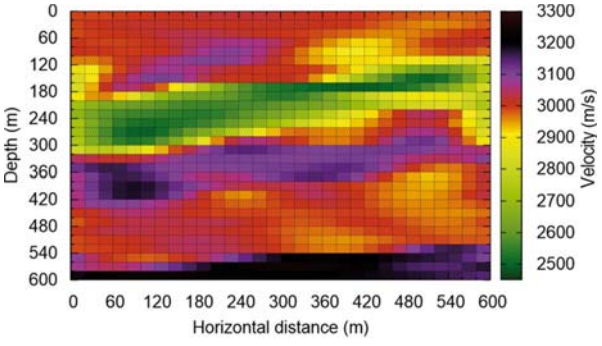

Figure 13 – Estimated model, linearized case, third stage with second order regularization and noise factor $\alpha = 0.010$.

Finally, in the fourth and final stage, after the last carbon dioxide injection step, the reservoir is homogeneously saturated with 60% fluid and 40% water (see Fig. 14). Thus, the entire reservoir layer has a single value seismic velocity of 2560 m/s. In both cases, linear and linearized, in the selection of singular values, as in the regularization, we obtain satisfactory results because it was possible to image the reservoir saturated with CO_2, despite the presence of noise (see Figs. 15, 16 and 17).

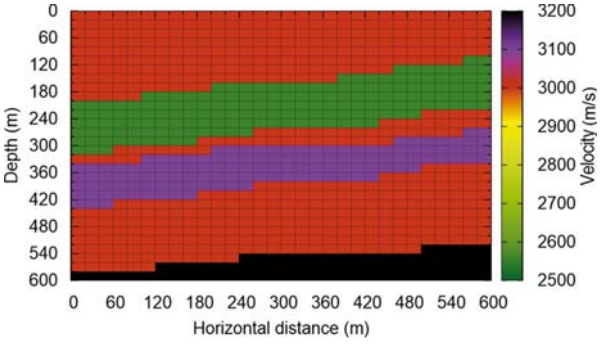

Figure 14 – True model, fourth stage with 60% saturation of CO_2 in the reservoir of interest.

CONCLUSIONS

When addressing fluid replacement, Gassmann's equation is an useful tool that can model the change of velocity within the reservoir. Based on the results obtained by the Gassmann's equation, traveltime seismic tomography was implemented.

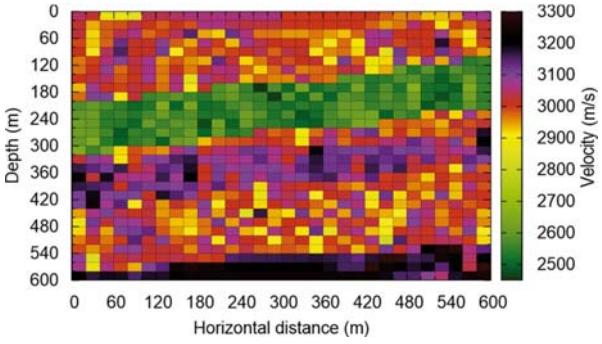

Figure 15 – Estimated model, linear case, fourth stage with 658 singular values and noise factor $\alpha = 0.010$.

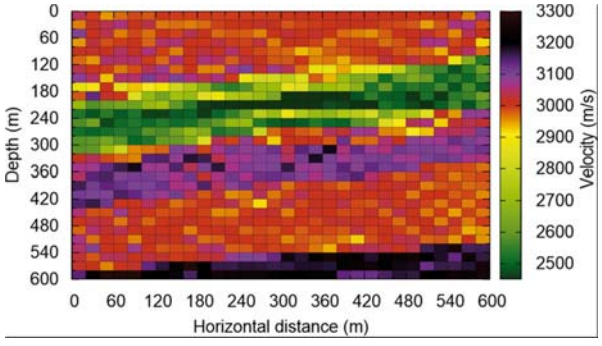

Figure 16 – Estimated model, linearized case, fourth interaction of the fourth stage with 300 singular values and noise factor $\alpha = 0.010$.

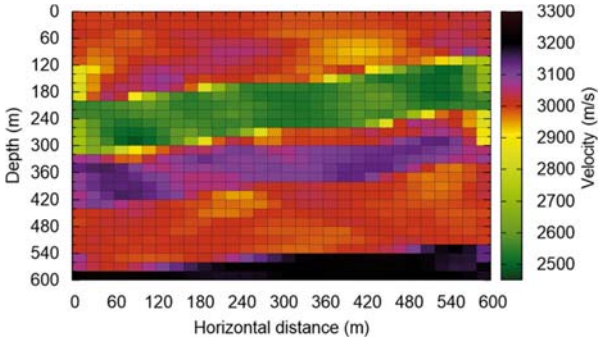

Figure 17 – Estimated model, linear case, fourth stage with first order regularization and noise factor $\alpha = 0.010$.

Seismic tomography has two important aspects for geological analysis: the estimation of properties and imaging. Thus, tomography results in a widely applicable tool in geophysics; however, it is an ill-posed, inverse problem and certain mathematical treatments are needed to provide the reliable solutions. For this purpose, the method of selection of singular values and the regularization by derivative matrices were applied.

Traveltime seismic tomography has proven to be a useful tool for monitoring CO_2 injection in sandstone reservoirs because it is

possible to verify the migration of fluid in the reservoir due to velocity variations in several stages for the linear and linearized case, which can satisfactorily define the entire region in which the fluid is located. For the proposed problem, the use of ray theory with the appropriate model discretization is viable due to the absence of abrupt changes of velocity, although a small energy dispersal is noted. The results of simulations, which included noisy data, were satisfactory in dealing the ill-conditioning of the inverse problem.

ACKNOWLEDGMENTS

L.R. Pereira thanks CAPES for the M.Sc. scholarship. A. Bassrei thanks CNPq for the project 308.690/2013-3 (research fellowship), CNPq and PETROBRAS for their support of the National Institute of Science and Technology of Petroleum Geophysics (INCT-GP), and FINEP for its support of the Research Network in Exploration Geophysics (Rede 01).

Recebido em 10 agosto, 2015 / Aceito em 10 abril, 2017
Received on August 10, 2015 / Accepted on April 10, 2017

REFERENCES

ANDERSEN AH & KAK AC. 1982. Digital ray tracing in two-dimensional refractive fields. Journal of Acoustical Society of America, 72(5): 1593–1606.

MENKE W. 1989. Geophysical Data Analysis: Discrete Inverse Theory. 2nd ed., Academic Press, San Diego, CA, 289 pp.

RAVAGNANI ATFSG & SUSLICK SB. 2008. Modelo dinâmico de sequestro de CO_2 em reservatórios de petróleo. Revista Brasileira de Geociências, 38: 39–60.

SCHOTS HA. 1990. Tomografia Sísmica Poço a Poço e Poço a Superfície utilizando Ondas Diretas. Master Dissertation, Universidade Federal da Bahia, Salvador, Brazil, 81 pp.

SMITH TD, SONDERGELD CH & RAI SC. 2003. Gassmann fluid substitutions: A tutorial. Geophysics, 68: 430–440.

WANG ZZ. 2001. Fundamental of rock physics. Geophysics, 66: 398–412.